Environ. Sci. Technol. **1999**, *33,* 4318−4325

Analysis of Hydrocarbons and Ash Particles Formed from Contaminated Industrial Biowaste under Combustion-like Conditions

JANUSZ A. KOZIŃSKI* AND GUOHUI ZHENG

Department of Metallurgical Engineering, McGill Metals Processing Centre, McGill University, 3610 University Street, Wong Building, Room 2160, Montreal, Quebec, Canada H3A 2B2

VIC ULOTH

Pulp & Paper Research Institute of Canada, 2711 Pulp Mill Road, Prince George, British Columbia, Canada V2N 2K3

PETER GANGLI†

FE 2000 Inc., 1000 Avenue Roche, Suite PH8, Vaudreuil, Quebec, Canada J7V 8P5

WES HUTNY

Natural Resources Canada, CANMET Energy Technology Centre, 555 Booth Street, Ottawa, Ontario, Canada K1A 0G1

A concept of multizone combustion of pulp and paper-generated biowaste was investigated. The biowaste was initially fed into the low-temperature region (<1250 K) and then subjected to the high-temperature treatment (1770 K), which was followed by sudden quenching in a second low-temperature zone (≪1250 K). This type of burning is called the low−high−low temperature process (LHL). It was found that destruction of selected polycyclic aromatic compounds occurred during the LHL process before they were emitted into the atmosphere. The biowaste material underwent dramatic morphological changes, which influenced segregation of metals within ash particles and their leachability. The heavy metals (Cr, Cd, Pb) were encapsulated and immobilized within the ash particle core surrounded by a compact shell consisting of condensed layers of light nonhazardous metals (Si, Al, Na, K). It seems that the multizone combustion of biowaste may be an attractive and useful way for the clean and efficient disposal of contaminated biowastes.

Introduction

To remain faithful to environmental covenants, many industrial sectors, e.g., pulp and paper and steel industries, are facing new challenges. They generate contaminated wastes that have to be disposed of. Combustion of wastes is a proven disposal technology that permits the reduction of hazardous material to a fraction of its original volume while generating energy (*1*, *2*). However, in the case of residues containing aromatic hydrocarbons and heavy metals (e.g., pulp and paper sludge, contaminated soil, or metallurgical slag), the transfer of these environmentally detrimental components into the combustion products is a major issue of public concern (*3*, *4*).

In this paper, the focus is on toxic heavy metals and polycyclic aromatic compounds (PACs) that cannot be captured by the classical air pollution control equipment. Many PACs are carcinogenic. Therefore, even fractionally small emissions of PAC may become substantial health hazards. These hydrocarbons are often present in the vapor phase, subsequently condensing onto fine particles. These particles also contain heavy metals released during combustion (*5*). Thus, the fine particles may act as carriers of both the PACs and toxic metals.

As particle−PAC−heavy metal aerosol is known to be mutagenic to bacterial and human cells (*6*), research directed toward their formation and destruction is of interest to public health officials and industries generating contaminated wastes. It is particularly meaningful when residual materials containing aromatic hydrocarbons and toxic metals are burned. Such residual materials are often generated during biological treatment of industrial solid wastes. The residues, which are left after the biological treatment, are called biowaste. They are still hazardous and have to be treated prior to their disposal. Most of these residues (e.g., pulp and paper sludges) contain enough combustibles to be considered as low-grade fuel surrogates. Because of the energy conservation and waste management problems, it is possible that in the future more low-grade fuels will be used. All in all, it is important to collect and interpret data related to the properties of biowaste material in the high-temperature environment existing during combustion.

In this research, a multizone temperature concept, shown in Figure 1 (bottom), was applied to dispose of biowastes. In this method, the biowaste is initially fed into the low-temperature region (<1250 K) and then subjected to the high-temperature treatment (1770 K), which is followed by sudden quenching in a second low-temperature zone (≪1250 K). This type of burning process will be called the low−high−low temperature process (LHL).

Experimental Section

Apparatus. The experiments simulating events occurring during the LHL process were conducted in a computer-controlled facility consisting of a high-temperature Cahn TG-171 thermogravimetric furnace with maximum sample size of 100 g coupled with a Mattson Galaxy 5020 Fourier transform infrared spectrometer. This system has been described in detail elsewhere (*7*); therefore, only brief description is given here. Since the sample has to remain stationary inside the cylindrical ceramic crucible (15 mm diameter) placed in the combustion chamber (30 mm diameter), biowaste "movement" through the LHL regions was simulated by programming the temperature ramps as illustrated in Figure 1 (top). The facility can relatively closely simulate the residence time, temperature histories, and chemical environment of commercial waste remediation units allowing for a variety of solid−solid, solid−metal, and solid−gas interactions. Changes in the sample weight and temperature as well as the gas composition inside the furnace are measured continuously. The reactor is designed for operation at atmospheric pressure with the temperature limit of 1970 K. The length of the heated zone is 300 mm with a homogeneous temperature zone of 100 mm (in this zone the radial temperature profiles are uniform). The extent and

* Corresponding author e-mail address: jkozin@po-box.mcgill.ca; fax: (514)398-4492; tel.: (514)398-2432.

† Current address: National Utility Investors, 1760 Fortin Blvd., Laval, Quebec, Canada H7S 1N8.

10.1021/es990087s CCC: $18.00
Published on Web 10/28/1999

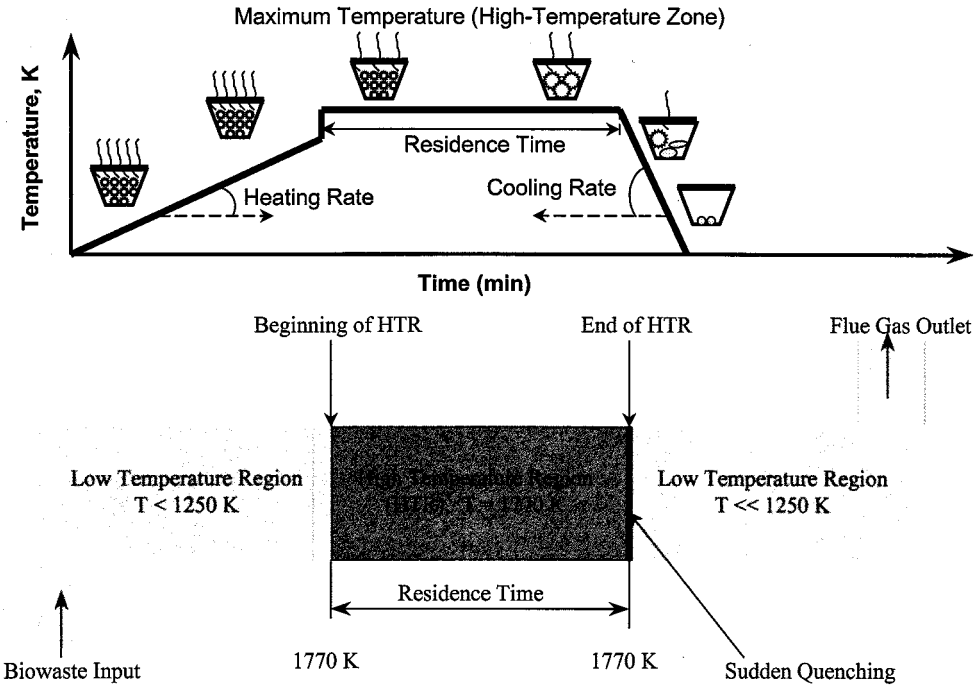

FIGURE 1. Illustration of a multizone temperature concept (bottom). In this low−high−low temperature (LHL) approach, biowaste is fed into the low-temperature region (<1250 K), then subjected to high-temperature treatment (1770 K) in the high-temperature region (HTR), which is followed by another low-temperature region (≪1250 K). Movement of the biowaste through the LHL regions was simulated by programming temperature ramps in the thermogravimetric furnace (top).

TABLE 1. Physicochemical Properties of Biowaste Residues

Ultimate Analysis (wt %)			
carbon	40.10	moisture	10.00
hydrogen	2.11	nitrogen	0.60
sulfur	0.10	oxygen	26.72
ash	20.37		
Proximate Analysis (wt %)			
volatile matter	6103	mineral matter	20.37
fixed carbon	860	moisture	10.00
heating value	15800 kJ/kg		
Ash Elemental Analysis (wt %)			
SiO_2	5647	Na_2O	1.40
Al_2O_3	29.43	K_2O	0.61
CaO	4.49	Fe_2O_3	0.96
TiO_2	3.11	P_2O_5	0.14
MgO	2.92	SO_3	0.47
Selected Metals Identified in the Biowaste (ppm)			
Si	49000	Cd	2430
Al	29500	Pb	2800
Ca	6200	Cr	2780
Na	2000		
PACs added to the Biowaste			
fluorene		cyclopenta[*cd*]-pyrene	
phenanthrene		benzo[*a*]pyrene	

location of the homogeneous zone was determined in the presence of both the sample and the air flowing within the reactor. Data are collected on-line using an ATI−Cahn−Mattson data acquisition system.

Materials. The biowaste used in this research was initially generated by a pulp and paper mill employing a deinking process. It was subsequently biologically treated with *Leptospirillum* bacteria. The biowaste studied was thus a solid residue that remained in a pond after biological processing of the deinking waste. The appearance and properties of the biowaste are shown in Figure 2 and listed in Table 1, respectively. The biowaste consisted mainly of hydrocarbons (61.03%), oxygen (26.72%), ash (20.37%), and moisture (10.00%). Small, as for the industrial biowaste, quantities of nitrogen (0.60%) and the absence of detectable quantities of sulfur suggest that fuel NO_x and SO_x emissions should not be of concern in this case (*8*).

Individual irregular fragments of the biowaste (5−25 mm) were composed of long cylindrical fibers with diameters between 15 and 50 μm and lengths between 200 and 500 μm (see Figure 2). The fibers were intertwined with each other and randomly distributed with no preferential alignment. Fine fibers (diameter <20 μm) made up the bulk of the biowaste matrix, while large fibers (diameter >30 μm) were trapped inside the matrix. The matrix appeared rather dense and nonuniform in comparison to the individual fibers.

The heating value of the biowaste was 15.8 MJ/kg, which is higher than the typical heating value of municipal solid waste and about half that of bituminuous coal (*9, 10*). Ash elemental analyses showed a dominance of SiO_2, Al_2O_3, and CaO (56.47%, 29.43%, and 4.49%, respectively) with high levels of alkalis ($Na_2O + K_2O$ > 2.00%). The biowaste was doped and well mixed with lead, cadmium, and chromium. Aqueous solutions of metal nitrates such as $Cr(NO_3)_3 \cdot 9H_2O$, $Cd(NO_3)_2 \cdot 4H_2O$, and $Pb(NO_3)_2$ were used. They were mixed with the biowaste at a known mass ratio, using enough water to completely saturate them. After being mixed for 1 h, the biowaste particles were dried overnight at 380 K. Water was then added back to the waste to a level of 10.0 wt %. The final concentration of lead was 2800 ppm, cadmium was 2430 ppm, and chromium was 2780 ppm. Both the added metals (Cd, Cr, Pb) and metals naturally present in the ash (Si, Al, K, Na) were randomly dispersed inside the feed biowaste after it was doped with heavy metals and prior to combustion (*11*). In addition, no influence of biomass predrying and rehydration on combustion profiles was observed (*12*).

Since it was important for this study to determine the concentrations of PACs during the combustion of the solid residues, the biowaste was also enriched with selected PACs, namely, fluorene, phenanthrene, cyclopenta[*cd*]pyrene and benzo[*a*]pyrene, were added (see Table 1).

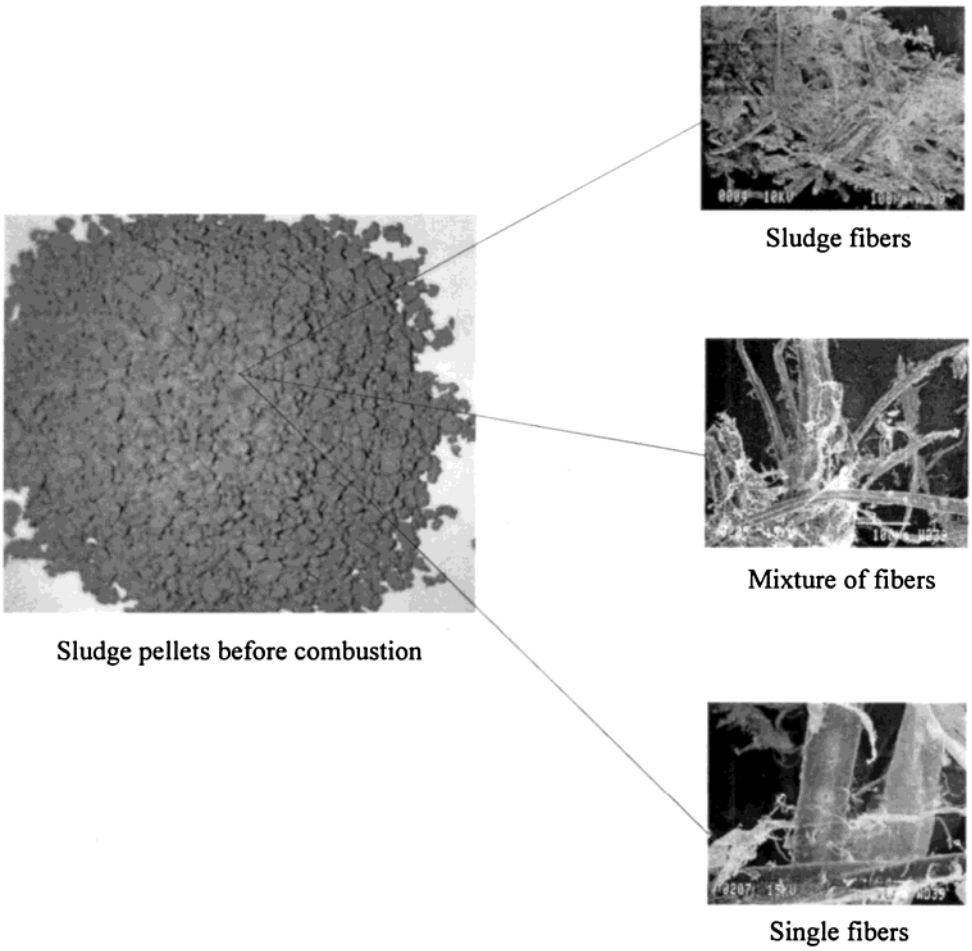

FIGURE 2. Morphological characteristics of the biowaste material prior to combustion.

Experimental Design. The morphology/topography of ash particles formed during biowaste burning, distributions of metals inside ash particles, and concentration profiles of polycyclic aromatic compounds were determined. Data were obtained during the experiments when a 50-g sample of biowaste residue was heated to 1770 K at an average rate of 50 K/min, then held in this high-temperature zone for 300 s, and subsequently quenched in liquid nitrogen outside the furnace (~14 000 K/min). These conditions were found to be optimal to significantly reduce the potential environmental impact of the biowaste treatment (*13*). The temperatures for the three LHL zones (maximum temperature of 1770 K; and low temperatures below 1250 K) were chosen to ensure that ash formed during combustion will be present as a molten material inside the high-temperature region (the ash deformation point was at ~1400 K) and that it will solidify upon entering the low-temperature region. The heating and quenching rates as well as the influence of the crucible location, sample condition, and gas flow on the measurements were carefully verified in separate experiments (*14, 15*). The temperature within the combustion chamber was measured with a B-type microthermocouple, which responded quickly to the changes of the conditions within the furnace (e.g., drying, pyrolysis, and burning of the biowaste). Thus, the reported heating rate was determined on the basis of the true temperature history rather than simply from the programmed temperature ramps. To achieve waste combustion, a continuous flow of air (120 mL/min) was delivered to the reactor. The air flowed around a ceramic crucible in which the biowaste was placed, first entering at the top of the sample. Oxygen diffusion was from the top to the bottom of the sample. Thus, the sample was burned in a layered mode. Because the combustion process was not occurring in the bulk volume of the biowaste sample, as it usually occurs in large-scale practical combustion units, we refer to the process as taking place under combustion-like conditions. Both the radial and axial temperature profiles as well as gas flow patterns were held uniform around the sample located inside in the homogeneous zone.

Instrumental Methods. The solid samples were analyzed to determine ash morphology, size, surface characteristics, and composition. The polished cross-sections of the ash particles embedded in epoxy were used for particle interior analysis. Filter-dispersed samples were used for surface analysis. Analyses were performed using a JEOL 8900 SuperProbe electron probe microanalyzer (EPMA) equipped with five wavelength-dispersive spectrometers (WDS) and a Noran energy-dispersive X-ray spectrometer (EDS). The WDS/EDS spectrometers were used to determine concentrations/distributions of the following metals: Si$K\alpha$, Al$K\alpha$, Na$K\alpha$, K$K\alpha$, Cd$L\alpha$, Pb$M\alpha$, and Cr$M\alpha$. Measurements of all the elements were conducted at 100 s counting times, 20 keV accelerating voltage, and 100 nA beam current. The standard and unknown samples were coated with carbon simultaneously to ensure an equivalent thickness of the carbon coat. The same counting time was used for standardization so that any effects of C contamination in the sample chamber would be similar for the standard and for the unknowns. The EPMA operated in the backscattered, secondary, or absorption electron imaging modes. In some cases, EDS was used together with WDS allowing the simultaneous acquisition of major, minor, and trace element data.

The measured metal contents (e.g., Cd > 400 ppm, Pb > 450 ppm) were much greater than their corresponding limits

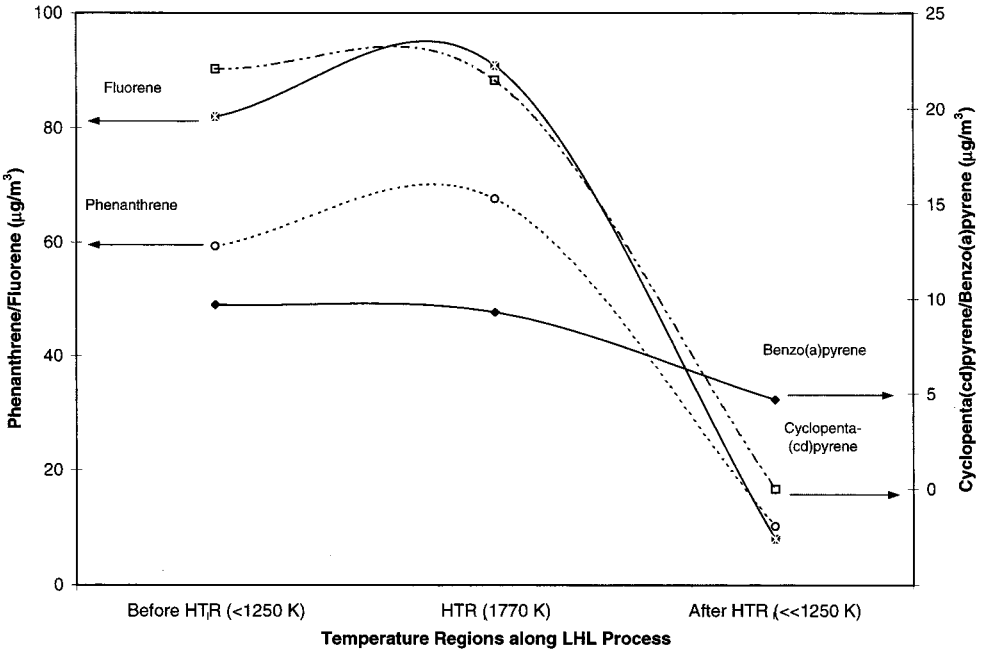

FIGURE 3. Concentration profiles of fluorene $C_{13}H_{10}$, phenanthrene $C_{13}H_{10}$, benzo[*a*]pyrene $C_{22}H_{12}$, and cyclopenta[*cd*]pyrene $C_{18}H_{10}$ along different temperature regions (HTR indicates the location of the high-temperature region in the LHL process).

of detection (*16*). To provide a representative statistical distribution, at least 3000 ash particles were examined in each individual sample. Ash and sludge microphotographs were taken at magnifications varying from 252 to 110 000 times to minimize "losses" of small particles in the background. Inaccuracy in the EPMA measurements is typically within a 5−7% range (*17*).

Leachability of metals from ash particles was determined with tests similar to the Toxicity Characteristics Leaching Procedure (*18*). A 0.5 M acetic acid solution was added to the ash samples at a solid-to-liquid ratio of 1:10 and mixed for 24 h. The concentrations of heavy metals in the filtered liquid were analyzed using a Perkin-Elmer 3110 atomic absorption spectrometer.

Polycyclic aromatic compounds (PACs) were identified by a Mattson Galaxy 5020 FTIR and quantified by a Varian Saturn 3 gas chromatograph−mass spectrometer (GC−MS). Gas samples containing major combustion gases (CO_2, H_2O, O_2, CO) and PACs were collected using a quartz sampling probe (0.8 mm diameter), the tip of which was located just above the sample container allowing for the withdrawal of undiluted gas samples for analyses. The gas sampling was accomplished via a heated glass sampling line (470 K) in order to avoid catalytic reactions that could form PACs on surface between 520 and 570 K. Gas-phase time-resolved concentration profiles were obtained. The gas phase IR spectra were obtained using a 160-cm-long gas cell-transfer line assembly equipped with wide band MCT detector with linearized, low-noise preamplifier. Detector bias current was optimized for maximum sensitivity operation at 77 K. The spectral range was analyzed from 7800 to 400 cm^{-1}. Typically 100 scans were co-added for each spectrum at a nominal resolution of 2.0 cm^{-1}. PACs were recognized on the basis of the IR spectra and response factors obtained for each PAC, which were compared with those of standard compounds (NIST-EPA Gas-Phase Infrared Database was used).

GC−MS analyses were performed on solid particles and high boiling PACs collected in an ORBO-100 charcoal organic trap located inside the sampling line. Volatile analytes from the reactor were transferred into a fused silica capillary column (2.1 m long, 0.18 mm i.d.; coated with DB-1, 0.4 μm film thickness) located within the Saturn 3 GC−MS. The column was programmed to start at an oven temperature of 313 K, where it remained for 500 s. The temperature then rose to 673 K at a rate of 2 K/min and was maintained at this final temperature for 300 s. The mass spectrometer was scanned from *m*/*z* 34 to *m*/*z*350 at a 2 scan/s rate. The mass spectra, registered at 70 keV, were obtained automatically during the chromatographic analysis. Most spectra were recorded on a rising total ion current curve (the best mass spectra). When the peaks in the chromatogram were not distinctly separated from one another, the spectra were recorded at the peak tops. Individual PACs were identified on the basis of relative retention times, mass spectra, and response factors obtained for each PAC, which were compared with those of standard compounds. PAC concentrations ($\mu g/m^3$) were calculated using flue gas flow rate and ion count area data obtained in these experiments as well as information from earlier experiments (*19, 20*). The total PAC concentrations were calculated by summing the concentrations of individual PACs.

Results and Discussion

Distribution of Polycyclic Aromatic Compounds. Temperature-resolved profiles of polycyclic aromatic compounds (PACs) identified during the combustion experiments of the biowaste are shown in Figures 3 and 4. The PACs concentration is plotted against the position along the low−high−low temperature regions. Measurement points for the PAC concentrations were located at the entrance of the high-temperature region (HTR) and inside the low-temperature regions before and after the HTR (see Figure 1 for the location of the high-temperature region in the LHL process).

The general trend observed was that the PAC concentrations were significantly lower in the low-temperature region following the HTR than in the zones preceding it. The concentration of fluorene decreased from 90.9 to 8.0 $\mu g/m^3$ (Figure 3). The concentrations of phenanthrene, benzo[*a*]-pyrene (Figure 3), and fluoranthene (Figure 4) decreased from 67.6, 9.3, and 51.0 $\mu g/m^3$ to 10.2, 4.7, and 28.6 $\mu g/m^3$, respectively. Both cyclopenta[*cd*]pyrene (Figure 3) and coronene (Figure 4) were not detected at the furnace exit while their concentrations at the entrance of the HTR were 21.5 and 11.8 $\mu g/m^3$, respectively. The amount of retene decreased

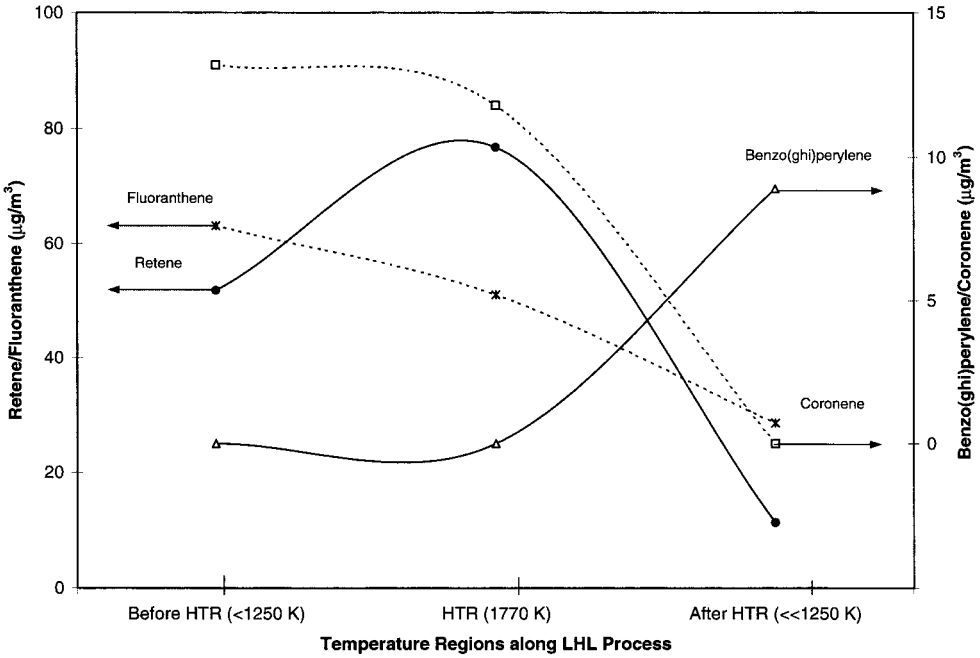

FIGURE 4. Concentration profiles of fluoranthene $C_{16}H_{10}$, retene $C_{18}H_{18}$, benzo[*ghi*]perylene $C_{22}H_{12}$, and coronene $C_{24}H_{12}$ along different temperature regions (HTR indicates the location of the high-temperature region in the LHL process).

from 37.4 to 11.1 $\mu g/m^3$ (Figure 4). The overall PACs reduction trend is confirmed by a 78.2% decrease in the total PACs from the initial concentration of 328.8 to the final 71.7 $\mu g/m^3$.

Some of the PACs detected during the combustion experiments were also found in the biowaste (e.g., fluorene and phenanthrene). Although some pyrosynthesis might be responsible for the formation of these species, it is unlikely that they would be formed in such high concentrations (90.9 and 67.6 $\mu g/m^3$, respectively). Therefore, the high concentrations of these species in the combustion gas, prior to and at the entrance of the HTR, could be attributed mainly to their presence in the biowaste.

Fluoranthene and coronene were not found in the biowaste. The relatively high concentrations of these species (51.0 and 11.8 $\mu g/m^3$, respectively) were likely a result of new fluoranthene and coronene molecules forming during decomposition of higher hydrocarbon compounds and interactions between lower hydrocarbons leading to the formation of larger and relatively stable molecules.

Mutagenic benzo[*ghi*]perylene was detected only in the low-temperature region following the HTR (Figure 4). This aspect of benzo[*ghi*]perylene behavior is still not clear and is difficult to explain by the present state of the analysis. However, it may be expected that benzo[*ghi*]perylene molecules were formed along the biowaste combustion pathway and that the formation mechanisms prevailed over those processes leading to benzo[*ghi*]perylene destruction.

1-Methyl-7-isopropylphenanthrene, known as retene, belongs to the alkylated phenanthrene compounds and is usually formed during smoldering combustion (*21*). Since retene was present in the gas samples, it implies that a period of low-temperature smoldering combustion takes place during biowaste burning. It is expected that retene was primarily formed by thermal degradation of resin compounds in the biowaste, a different formation mechanism than other PACs. This mechanism involves cracking of organic compounds to smaller, unstable molecules. These fragments, mostly radicals, recombine to larger aromatic ring systems by pyrosynthesis.

It is expected that the decrease in PACs concentration may be due to the release of hydroxyl radicals (OH) in the high-temperature region and subsequent PAC decomposition via OH oxidation (formation of aliphatic and paraffinic hydrocarbons was noticed). It is evident that the PAC destruction during the combustion of biowaste residues occurs within the LHL reactor before PACs are emitted into the atmosphere.

Ash Morphology and Surface Topography. Biowaste material underwent dramatic morphological metamorphosis during combustion, as illustrated in Figure 5. As the fibrous mixture (Figure 5A) was heated and oxidized (the ignition temperature was about 360 °C), small inorganic inclusions appeared sporadically in the form of irregular particles with sizes smaller than 10 μm. These particles formed chains replacing the initial fibers (Figure 5B). The oxidation reactions caused visible shrinking of the initial ash inclusions. At temperatures exceeding 1100 °C, it was clear that sintering of the ash particles occurred (Figure 5C). As indicated in Table 1, the ash consisted mostly of Si−Al−Ca compounds. The phase diagram of the $CaO-Al_2O_3-SiO_2$ ternary system suggests that it could be melted when the temperature reached or exceeded the ~1185 °C melting point for these compounds (*22*). Thus, most of the ash appeared as a liquid phase. Consequently, spherical particles were generated. They were attached one to another (see Figure 5C). When temperature reached 1400 °C, the ash was completely transformed into a molten phase. High temperature efficiently removed previously present structural differences. The structure of the ash heated to 1500 °C and subsequently quenched indicates that the ash has a smooth surface and is compactly built with high probability of a condensed internal structure (Figure 5D). It was confirmed (*13, 23*) that the ash particle has a nonporous, dense, and compact structure.

The observed profound changes in the particle morphology and surface topography should influence the properties of the biowaste−ash system that are important from an environmental point of view (e.g., leachability of toxic metals).

Distribution and Leachability of Heavy Metals. Metals associated with the biowaste−ash system were divided into three groups: (1) matrix metals (Si and Al), which constituted the bulk of the inorganic material (see Table 1); (2) heavy toxic metals (Cd, Cr, Pb), which are hazardous for the

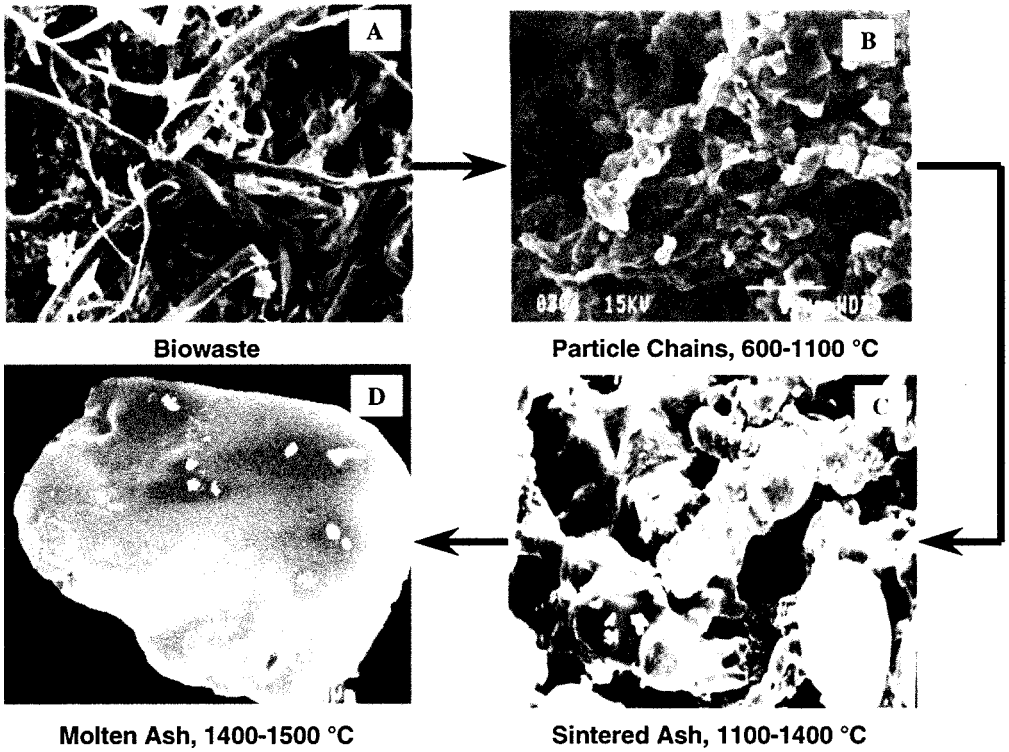

FIGURE 5. Morphological metamorphosis of the biowaste material under combustion-like conditions. (A) Biowaste at room temperature (average fiber size 30 × 350 μm). (B) Particle chains at 600−1100 °C (average chain size 15 × 100 μm). (C) Sintered ash at 1100−1400 °C (average particle size 50 μm). (D) Molten ash at 1400−1500 °C (average particle size 20 μm).

environment or human health; and (3) light alkali metals (Na, K), which significantly decrease the melting point of the ash. It was observed that the matrix metals were rather uniformly distributed inside the ash particles regardless of temperature (*13*). It suggests that the morphological changes did not influence significantly the behavior of the ash matrix metals. Contrary to Si/Al, combustion temperature and structure transformations were important for the distribution of heavy and light metals in the solid residue. At low temperatures (below 1000 °C), the concentrations of heavy metals in the particle core and in the surface region were comparable. Figure 6A shows the distribution of Pb in the core and on the surface of the ash particle collected at 900 °C (an area of 200 μm × 200 μm analyzed with EPMA−WDS). The amount of lead present in the core and the surface was 1435 and 1461 ppm, respectively.

At high temperatures (1250 °C and higher), there was a significant difference in Pb partitioning between the particle core and the surface. The concentration of lead on the surface at 1350 °C was only 163 ppm while total Pb detected in the core was 1212 ppm (Figure 6B). Similar behavior was observed for chromium and cadmium. At 900 °C, concentrations of Cr in the core and on the surface were 1410 and 1434 ppm, respectively; while at 1350 °C, 1316 ppm of Cr was measured in the core and 172 ppm was measured in the 5 μm thick surface layer. Cd was also almost uniformly distributed between the core and the surface at 900 °C (1342 and 1347 ppm, respectively). When temperature rose to 1350 °C, only 58 ppm of Cd was seen on the ash particle surface and 1319 ppm was seen within the particle core. It is clear that, during the LHL combustion, heavy toxic metals are partitioned within the ash particle core rather than on its surface. These findings are different from what was known from other studies on sludge and coal combustion (e.g., refs *24* and *25*). In these studies, it was shown that the conventional combustion yields ash particles with the surface predominance of potentially toxic elements such as Pb and Cr. These metals are easily leachable if located on the particle surface.

It should be mentioned that a bulk mass balance performed for the heavy metals (including also Ni, Zn, and Cu) indicated that 82.7% of the initial concentration of the heavy metals in the biowaste was retained in the ash particles. Thus, the ash particles generated during the multizone biowaste treatment under combustion-like conditions were capable of preventing a significant portion of the toxic metals from escaping into the flue gas stream.

The behavior of low-melting light alkali metals (Na and K) was also affected by temperature−ash morphology changes. They revealed the highest concentrations (almost 4.0%) in the regions close to the particle surface. This is opposite to the observed distribution of lead. It is illustrated in Figure 6C where the concentration of sodium at 1350 °C is significantly higher on the surface than inside the particle (3879 ppm vs 1682 ppm). Thus, in the final ash material light alkali metals were mostly located in the external surface and subsurface layers.

The leachability of the heavy metals from the final ash material was evaluated using the leaching index. It was defined as a percentage ratio between the mass of an individual heavy metal in the leachate and the initial mass of this heavy metal in the ash prior to leaching:

$$\mathrm{LI} = \frac{\text{mass of heavy metal in leachate}}{\text{initial mass of heavy metal in ash}} \times 100\%$$

Results from the leaching test for different metals are presented in Figure 7 as a function of temperature. Data indicate that the leachability of Cr and Cd from particles formed at temperatures below 1000 °C is relatively high. The leaching values for Cd and Cr are 1.5 and 5.9% for particles extracted at 750 °C, respectively, and 0.5 and 1.2% for particles formed at 900 °C, respectively. Since the initial concentration of Cr in the contaminated ash pellet prior to leaching was 8000 ppm, the results suggest that 472 ppm of Cr leached out from the particles formed at 750 °C. In the case of Cd, 32 ppm was found in the leachate (initial concentration of Cd

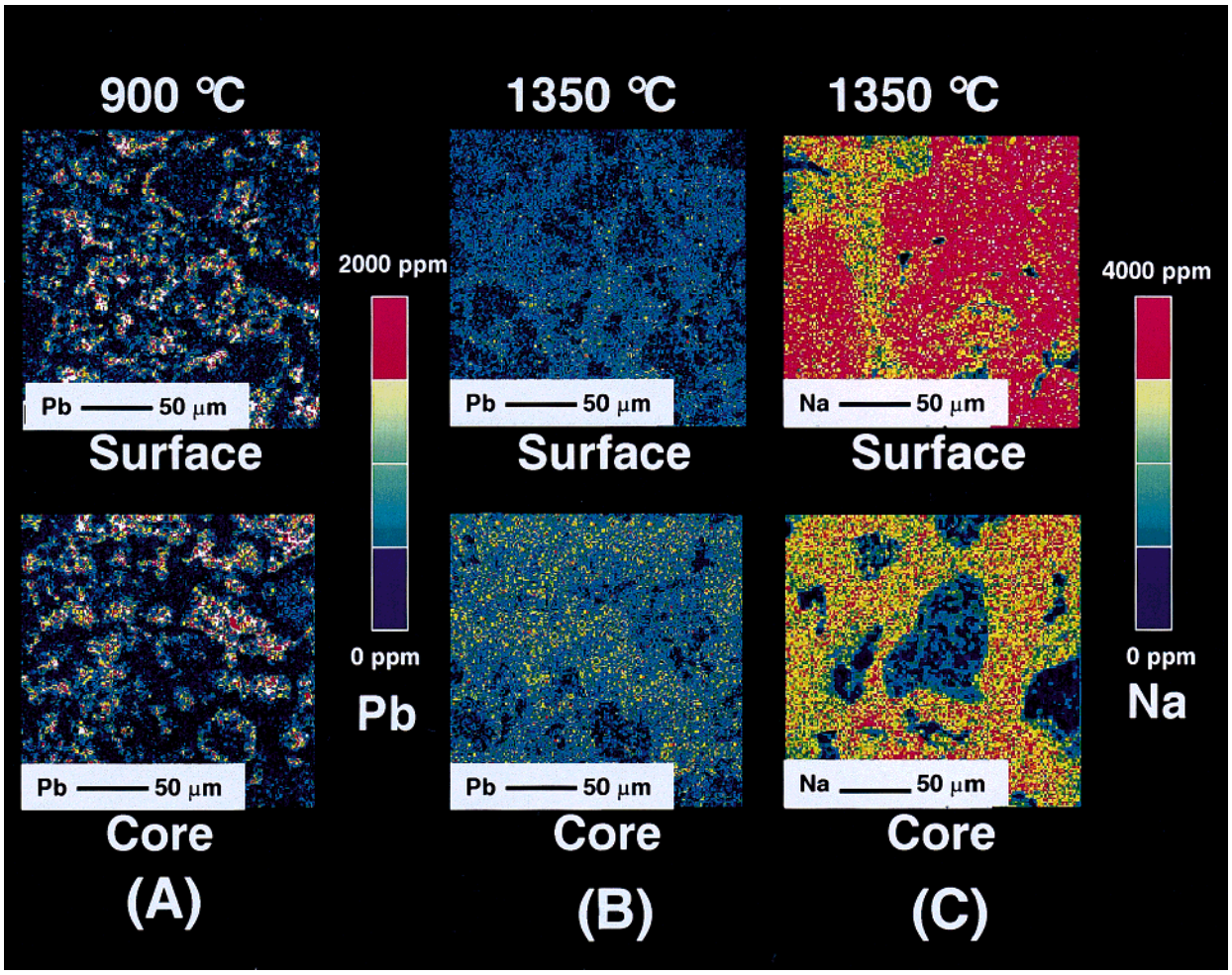

FIGURE 6. Distribution of heavy and light metals (Pb and Na, respectively) between the surface and the core of the ash particle collected at 900 and 1350 °C. (A) Distribution of Pb at 900 °C. (B) Distribution of Pb at 1350 °C. (C) Distribution of Na at 1350 °C.

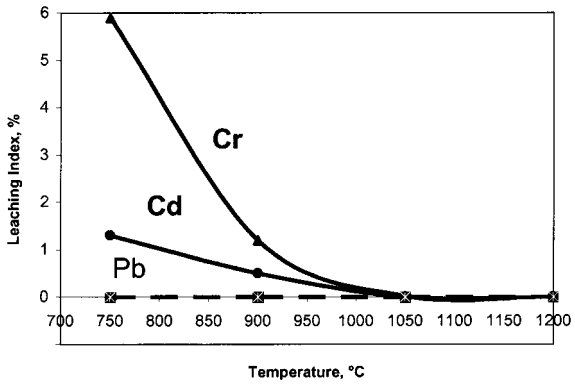

FIGURE 7. Influence of temperature on leaching of Pb, Cd, and Cr from the ash.

was 2140 ppm). No leaching of Pb was observed at low temperatures (initial concentration 152 ppm). As the particle formation temperature increased, the leaching rates for the heavy metals decreased. When the ash morphology changed into a dense material and the surface topography changed into a continuous and condensed substance (above 1200 °C), no toxic metals such as Cr, Cd, and Pb were detected in the leachate, probably due to fixation of heavy metals within the aluminosilicate matrix. No heavy metals in the leachate implies that compact ash particles formed at high temperatures could be safely disposed of (e.g., landfilled) or reused because such ash would not be classified as a hazardous material.

There is a question of what is the "driving force" for the observed behavior of metals during biowaste burning. It is expected that at low temperatures (below 1000 °C) metals are transported via diffusion within the initial inorganic solid matter. Light metals (e.g., Na and K) with low atomic radius and weight would easier pass through the fine pores within the ash particles than heavy metals (e.g., Pb, Cr, and Cd). Such a diffusion process could promote slight variations in metal concentrations inside the particle with light metals slightly enriched in the particle surface.

At higher temperatures (above 1250 °C) during ash melting, the primary mechanisms for mass transport are diffusion and viscous flow. The diffusion distance could be determined by cation patterns in the melt (*26*). It seems that the relative mobility of ash network formers (such as Si and Al) and network modifiers (such as Na and K) may control the nature of diffusion in a melt and may determine how metallic elements migrate (*26, 27*). Metallic elements are usually classified into four groups with respect to diffusion: (i) alkali ions (Na, K); (ii) network modifiers other than alkalis, mostly divalent cations (Ca, Mg, Pb, Cr); (iii) network forming cations (Si, Al, Ti); (iv) oxygen and other anions. The alkali ions have the simplest diffusion behavior among all species. A typical diffusion rate at 1300 °C is approximately 10^{-9} m^2/s in a silicate melt (*26*). Their diffusion rates are, in general, much faster than that of all other nonvolatile species. A typical diffusivity of other network modifiers such as Pb and Cr is about 10^{-11} m^2/s at 1300 °C in a silicate melt. It decreases with increasing silica content. Thus, in this study, the diffusivity of Pb^{2+}/Cr^{3+} is significantly lower than that of $K^+/$

Na^+ and would promote metals segregation in the ash.

Therefore, Na and K may rather easily move to the exterior of the ash particle while heavy metals (e.g., Cr) would be forced into the particle core area. Because the subsequent particle quenching process is very fast (~14 000 K/min), no rearrangements of heavy metals within the solidifying ash material are possible. As a result, the heavy metals seem to be encapsulated and immobilized within the ash particle core surrounded by a compact shell consisting of condensed layers of light nonhazardous metals.

The multizone combustion of biowaste in which sequential low−high−low (LHL) temperature regions are applied can be considered as an attractive and useful way for the clean and efficient disposal of contaminated biowastes due to the following reasons:

(i) It is possible to control ash particle structure, distribution of metals within ash, and destruction of selected polycyclic aromatic compounds in the LHL process. In fact, our data illustrate for the first time that toxic metals (Pb, Cr, Cd) are encapsulated within the ash particle core rather than located on the surface. In addition, they are immobilized (no leachability detected in ash particles treated at high temperature).

(ii) Environmental impact will therefore be reduced since nonhazardous ash, which is yielded in the LHL process, can be safely disposed of or reused.

Acknowledgments

The authors gratefully acknowledge financial support from the Natural Sciences and Engineering Research Council of Canada (NSERC Grants STP-0201954, OGP-0170464, and EQP-0173628), PAPRICAN, CANMET, and FE 2000, Inc. We also thank Glenn Poirre from McGill University for conducting EPMA-WDS analyses.

Literature Cited

(1) Niessen, W. R. *Combustion and Incineration Processes: Applications in Environmental Engineering*; Marcel Dekker: New York, 1995; pp 1−4, 112−171.
(2) Brunner, C. R. *Hazardous Waste Incineration*; McGraw-Hill: New York, 1993; pp 51−73.
(3) Wendt, J. O. L. *Twenty-Fifth Symposium (International) on Combustion*; The Combustion Institute: 1994; pp 277−289.
(4) Seeker, W. R. *Twenty-Third Symposium (International) on Combustion*; The Combustion Institute: 1990; pp 867−885.
(5) Kozinski, J. A.; Zheng, G.; Saade, R.; Di Lalla, S. *Can. J. Chem. Eng.* **1997**, *75*, 113−120.
(6) Braun, A. G.; Pakzaban, P.; Toqan, M. A.; Beer, J. M. *Environ. Health Perspect.* **1987**, *72*, 297−303.
(7) Saade, R.; Kozinski J. A. *J. Anal. Appl. Pyrol.* **1998**, *45*, 9−22.
(8) Figueroa, C. M. *Toxic Air Pollutant Emissions from Wood Pulp Mills & Waste Boilers*; NCASI Special Report 94-11; NCASI: 1994; pp 159−161.
(9) Zheng, G.; Kozinski, J. A. *Environ. Prog.* **1996**, *15*, 283−292.
(10) Thompson, C. G. *Recycled Papers: The Essential Guide*; MIT Press: Cambridge, MA, 1992; pp 21−47.
(11) Kozinski, J. A.; Saade, R.; Zheng, G. *Twenty-Sixth Symposium (International) on Combustion*; The Combustion Institute: 1996; pp 2495−2502.
(12) Zheng, G.; Kozinski, J. A. *Fuel* (in press).
(13) Kozinski, J. A.; Zheng, G. *Twenty-Seventh Symposium (International) on Combustion*; The Combustion Institute: 1998; pp 1745−1752.
(14) Di Lalla, S.; Kozinski, J. A. *J. Air Waste Manage. Assoc.* **1999**, *49*, 174−185.
(15) Zheng, G.; Di Lalla, S.; Kozinski, J. A. *Trans. Ind. Chem. Eng. Part B: Process Saf. Environ. Protect.* **1998**, *76*, 19−30.
(16) Scott, V. D.; Love, G.; Reed, S. J. B. *Quantitative Electron-Probe Microanalysis*; Ellis Harwood: New York, 1995; pp 103−142.
(17) Reed, S. J. B. *Electron Microprobe Analysis and Scanning Electron Microscopy in Geology*; Cambridge University Press: Cambridge, 1996; pp 89−114.
(18) Later, D. W.; Sorensen, G. *International Conference on Incineration & Thermal Treatment Technologies*, San Francisco, 1997; pp 12−16.
(19) Kozinski, J. A. *Combust. Flame* **1994**, *96*, 249−260.
(20) Kozinski, J. A.; Saade, R. *Fuel* **1998**, *77*, 225−237.
(21) Standley, L. J.; Simoneit, B. R. T. *Atmos. Environ. B* **1990**, *24*, 67−74.
(22) Wunsch, P.; Greilinger, C.; Bieniek D.; Kettrup A. *Chemosphere*, **1996**, *32*, 2211−2218.
(23) Ramesh, A.; Kozinski, J. A. *Appl. Surf. Sci.* (in press).
(24) Albertson, O. E. *Sludge Incineration: Thermal Destruction of Residues*; Manual of Practice FD-19; Water Environment Federation: Alexandria, VA, 1992; pp 295−309.
(25) Linton, R. W.; Williams, P.; Evans, C. A., Jr.; Natusch, D. F. S. *Anal. Chemistry* **1977**, *49*, 1514−1520.
(26) Frischat, J. *Ionic Diffusion in Oxide Glasses*; Trans. Tech. Publications: 1976; pp 13−23.
(27) Stebbins, J.; McMillan, F.; Dingwell D. B. *Mineral. Soc.* **1995**, *32*, 483−495.

Received for review January 25, 1999. Revised manuscript received September 20, 1999. Accepted September 20, 1999.

ES990087S